Chapter

Characteristic Aspects of Metal Wear: Wear-Induced Wear Transition and Characteristics of Wear Track Profiles

Naofumi Hiraoka

Abstract

This chapter describes two characteristic phenomena of metal wear that are usually not often considered but are related to the basic aspects of wear. The first is a mild-to-severe wear transition caused by the wear itself. Convex sliding pairs are usually accompanied by rolling sliding motion, but rolling sliding motion sometimes produces a peculiar wear profile, leading to high contact pressure. When the contact pressure exceeds a certain value that depends on the material, the wear mode changes to severe wear. This is a common wear transition for convex sliding pairs, but it can also occur for other pairs. The second is the similar appearance of wear tracks on various friction pairs. Rubbing metal under relatively severe conditions creates streaked wear tracks. We found the width and depth of these streaks, that is, wear track profiles are similar regardless of the sliding conditions and the material, which leads to similar appearance of the wear tracks. This suggests the existence of a general mechanism for producing wear tracks.

Keywords: wear track, roughness, profile, appearance, wavelet analysis, power spectrum density

1. Introduction

Two characteristic phenomena of metal wear are described in this chapter. The first is mild-to-severe wear transition [1, 2]. Severe-to-mild wear transition is usually observed in the running-in process. The transition is believed to be due to a smoothing of roughness [3], an increase in morphological conformity of sliding pairs due to wear [4], and/or oxide formation in the wear scars [5–8]. Mild-to-severe wear transition is sometimes observed in friction parts used for a long time. There are various causes of this transition. One of the simple causes is deterioration or depletion of lubricant [9]. Fatigue of the sliding surface or temperature increase [10] is also a possible reason.

We have found that convex sliding pairs, such as those used in some latch mechanisms or sliding electrical contacts, often cause the mild-to-severe wear transitions. This wear transition was found to be caused by an increase in contact pressure between the sliding pairs due to an increase in the wear shape inconformity of the sliding pairs. This wear shape inconformity was caused by the rolling-sliding motion of the convex sliding pair.

The second one is about wear track profiles [11, 12]. When metal sliding pairs are rubbed under relatively severe conditions, streaked wear tracks are generated in many cases. By observing the wear tracks of wear specimens which we have obtained for various test purposes and those of several published papers, we noticed that the appearance of many streaked wear tracks is similar. In other words, the width of the streaks does not change much regardless of the sliding material and wear conditions. We thought this suggests the existence of a general mechanism for producing wear tracks that can suggest the way to prevent severe damage from wear.

Though some researchers seemed to have been aware of this feature, few studies were found that focused on the wear track profile characterization [13], though many studies have been conducted on the wear scar or wear track morphology (e.g., [14]).

These two issues are often overlooked but we think they can be one of the key aspects of wear.

2. Wear-induced mild-to-severe wear transition

2.1 Experimental procedure

Figure 1 shows a schematic of the test rig. Semi-cylindrical upper specimen oscillatorily slides on the cylindrical specimen immersed in mineral oil [1, 2]. The lubrication condition is supposed to be boundary lubrication. This sliding motion is apparently a pure sliding but actually a rolling-sliding motion. **Figure 2** illustrates the specimen motion. The upper specimen rolls an angle of θ, while it slides a distance of R θ on the lower specimen. Note that usually the sliding direction is the same as the rolling direction in the rolling-sliding motion of a gear surface or a traction drive, but this rolling-sliding motion is opposite. Since both contact points of the upper and lower specimens move during sliding, it is more difficult to conform the sliding surface than pure sliding.

Test materials and test conditions are shown in **Tables 1** and **2**, respectively. The lower specimen was silver-plated in order to prevent the initial large contact

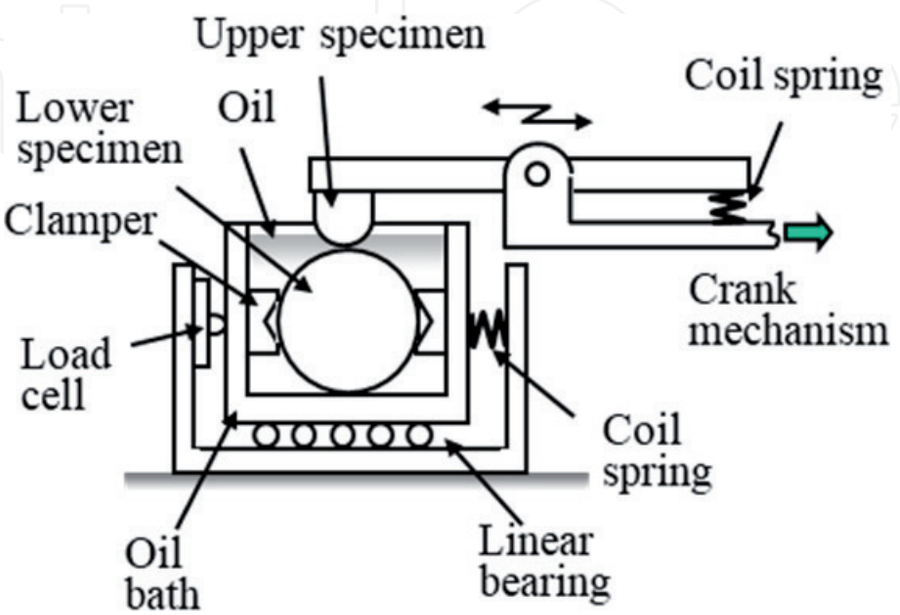

Figure 1.
Schematic of wear test rig [1].

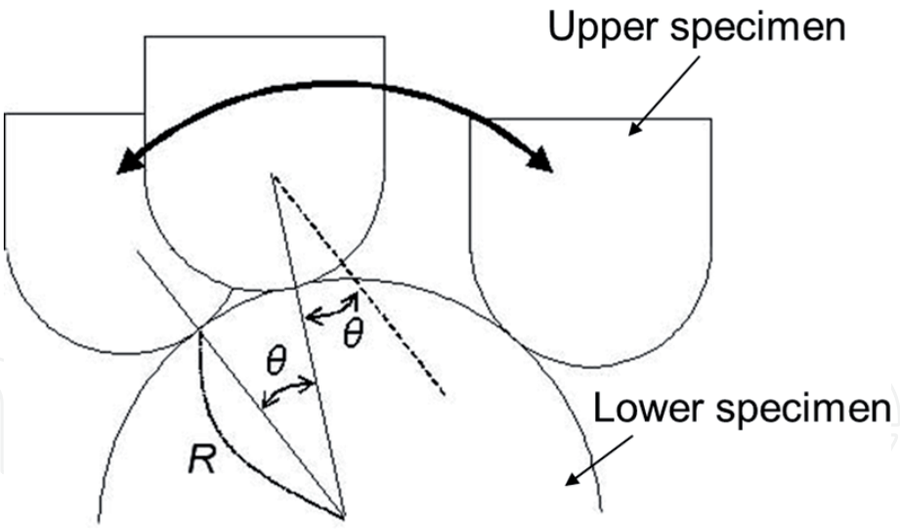

Figure 2.
Rolling-sliding motion of specimens [2].

Upper specimen	Radius; 3 mm, Width; 2 mm Material; 99.9% Cu (JIS C1100H, H_V ~100)
Lower specimen	Radius: 10 mm and width: 10 mm Material: 50 μm silver electroplated 99.9% Cu (JIS C1100H, H_V ~100)
Oil	Mineral and synthesized mixed insulating oil Kinetic viscosity: 5.2 cSt (40°C)

Table 1.
Test materials [1].

Motion	Oscillation
Atmosphere	Laboratory air (20 ~ 25°C, RH 40 ~ 60%)
Load (N)	39, 69, 83, 98
Frequency (Hz)	2
Stroke (mm)	10

Table 2.
Test conditions [1].

pressure due to misalignment. The load was applied by the coil spring. Loads shown in **Table 2** were those when the upper specimen was on top of the lower specimen. Therefore, the load varied during sliding by about 0 ~ −8% due to the vertical movement of the upper specimen. The horizontal force, that was the sum of the horizontal components of the friction and the load, was measured by the load cell to monitor the wear conditions.

2.2 Experimental results

Figure 3 shows the time evolution of horizontal forces. The forces shown were those of the maximum values for one oscillation. All forces indicated sudden increase except for the 39-N load. **Figure 4** indicates the trends of horizontal forces of the 69-N and the 98-N loads obtained from the tests of some oscillation numbers ((a)) and the wear depth at the center of the lower specimen wear scar of them ((b)).

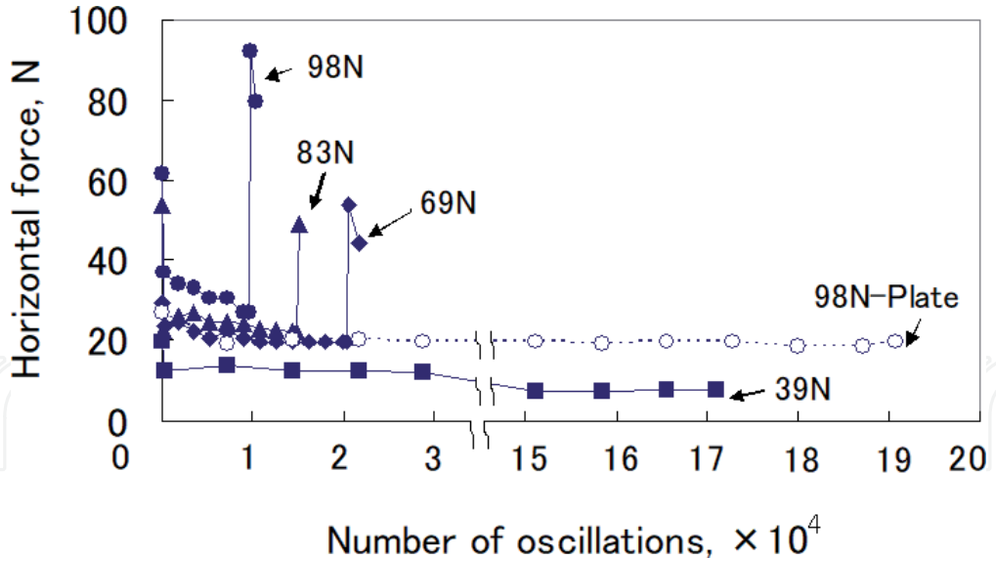

Figure 3.
Time evolution of horizontal forces for the loads tested [1].

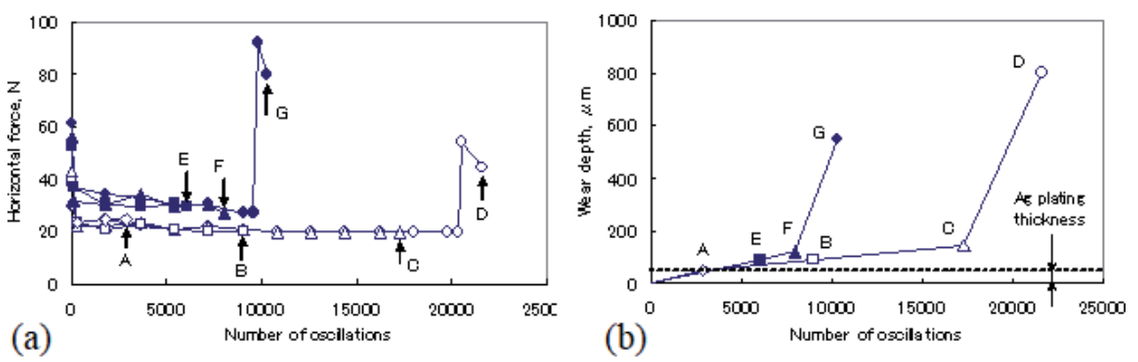

Figure 4.
(a) Trends of horizontal forces of the 69-N (empty symbols) and the 98-N loads (filled symbols) and (b) wear depth of lower specimen wear scar [1].

The wear depth gradually increased and then suddenly and rapidly increased at the oscillation numbers of sudden increase of horizontal forces (points G and D).

Figure 5 shows the microscope images of the wear scars of the lower specimens of B and D in **Figure 4**. From **Figure 5(b)**, the wear scar was rough and indicated the traces of hard adhesion, whereas that appeared relatively smooth in **Figure 5(a)**. From the wear depth progress in **Figure 4(b)** and wear scar appearances in **Figure 5**, the wear can be referred to as mild wear and severe wear before and after the sudden increase of the horizontal force, respectively. Thus, mild-to-severe wear transition occurred above a certain load.

Traces of silver-plating were not observed in **Figure 5**. **Figure 6** indicates the Auger electron energy intensity measured in the wear scars of the lower specimen of the tests stopped before (15,600 oscillations) and after (18,600 oscillations) the point C in **Figure 4** of 69-N load. No silver was detected in **Figure 6** which indicates that the silver-plating was depleted in the early stage of wear and was not related to the wear transition. The intensity of oxygen (O1) was almost the same for two specimens in **Figure 6**. This suggests that surface products of oxide were also not related to the wear transition.

Figure 7 shows the relations between the loads and the oscillation numbers of mild-to-severe wear transition points. It looks like the S-N curve for metal fatigue, indicating the possibility of fatigue as the cause of the wear transition. However,

Figure 5.
Optical microscope images of wears of lower specimens: (a) B and (b) D in ***Figure 4*** *[1].*

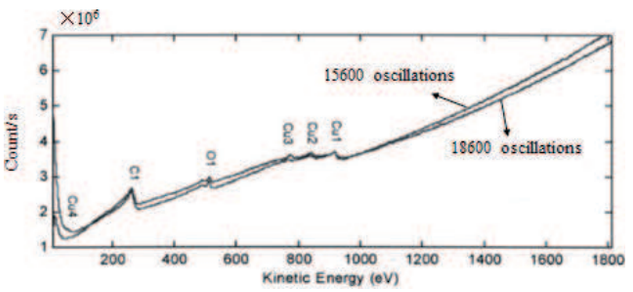

Figure 6.
Auger electron energy intensity in wear scars of lower specimen for 69-N load [1].

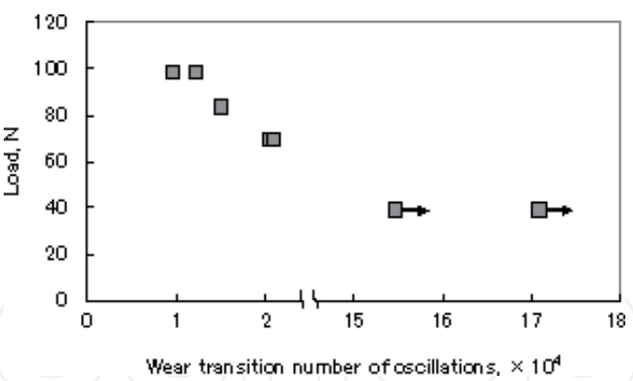

Figure 7.
Relations between loads and oscillation numbers of mild to severe wear transition points [1].

when pure sliding tests of 98-N load were carried out using the same upper specimens and the flat plates, the result is shown in **Figure 3**, no wear transition was observed. The Hertzian contact pressure calculated without considering the silver plate for the flat plate was 529 MPa, which was larger than that for cylindrical lower specimen of 69-N load: 504 MPa. The tests were conducted twice and almost the same results were obtained. This suggests that the fatigue was not the case for cylindrical sliding pairs.

Figure 8 indicates the temperature trend of the upper specimen under 69-N load. The temperature was measured with a thermocouple 1 mm above the contact point. The temperature was almost constant at around 25°C and was not the cause of the wear transition.

2.3 Discussion

The experimental results above indicate that the mild-to-severe wear transition was not due to the lubricant depletion, fatigue, or temperature rise. **Figure 9** shows the wear shapes of the upper and the lower specimens of 69-N load and 18,600 oscillations, measured along the circumferential direction at the center of the wear scar. The trapezoidal wear shape was generated by wear from the original circumferential shape. This peculiar wear shape was probably due to the rolling-sliding motion of the specimens, which made a contact shape inconformity and generated a large contact pressure.

To investigate the generation process of the peculiar wear shape and its effects on the contact pressure, wear simulations were conducted. Calculation model is shown in **Figure 10**. The contact pressure was approximated by the Hertzian contact pressure: $P(x)$. The contact area was divided into discrete slices of Δx width and the upper specimen moved byΔx in one calculation step. The wear depth was calculated by $KP(x)\Delta x$, where K was a virtual specific wear rate, and the new wear shape was obtained by smoothing the calculated discrete wear shape. The detail of the simulation was described in Refs. [1, 15–18].

The results of the simulations are shown in **Figure 11**. Calculation conditions are listed in **Table 3**. Materials for both specimens were supposed to be Cu with Young's modulus of 100 GPa and Poisson's ratio of 0.3. As shown in **Figure 11(a)**, the calculated wear shape reproduced the experimental result of the trapezoidal wear shape showing that the simulation can fairly simulate the wear phenomenon.

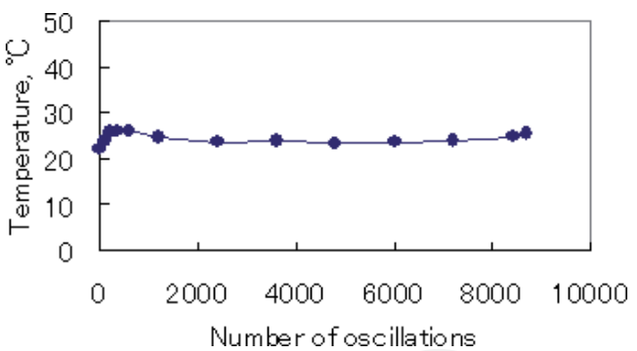

Figure 8.
Temperature trend of upper specimen under 69-N load [1].

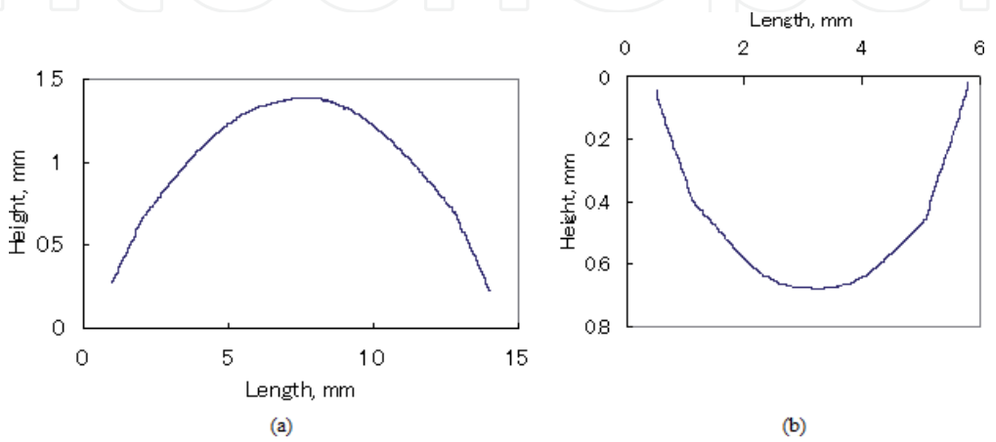

Figure 9.
Wear shapes of upper and lower specimens of 69-N load and 18,600 oscillations: (a) lower specimen and (b) upper specimen [1].

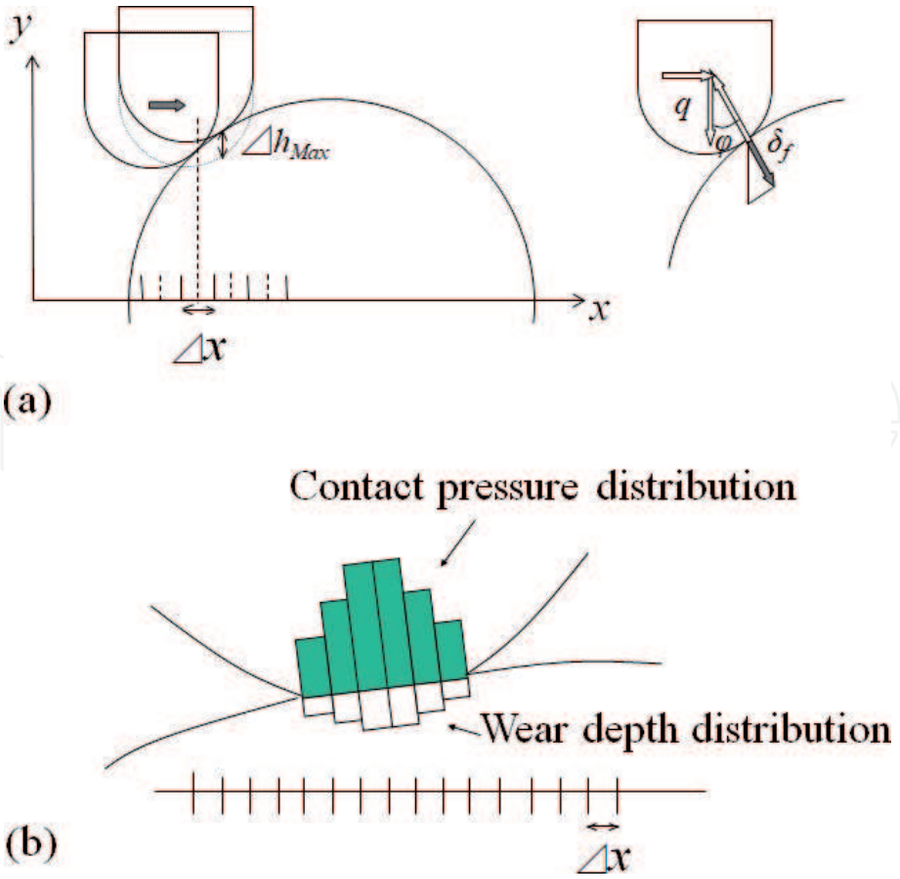

Figure 10.
Calculation model for wear simulation: (a) the whole of the model and (b) schematic of the contact area [1].

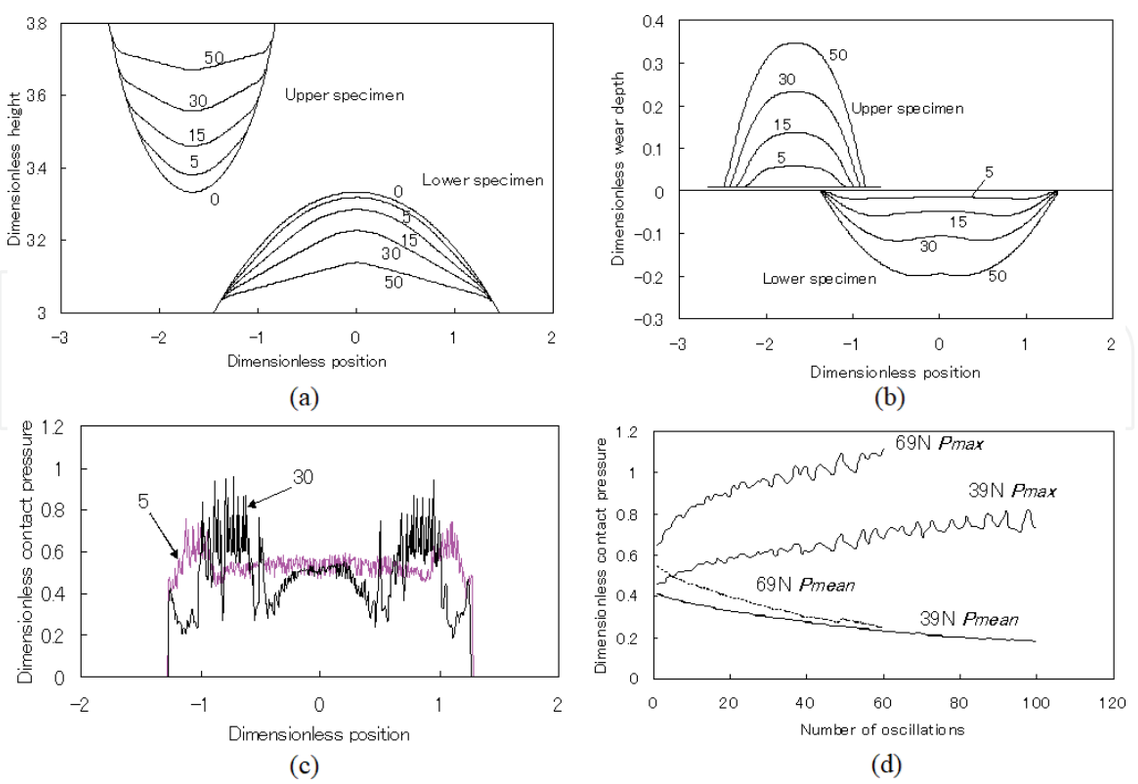

Figure 11.
Results of wear simulation for 69-N and 39-N loads: (a) specimen's shape change, (b) wear depth, (c) contact pressure on the lower specimen, and (d) time trends of the contact pressures (Pmax: maximum contact pressure, Pmean: mean contact pressure, for one oscillation) [1]. The length and the contact pressure were normalized by the upper specimen radius and hardness of the upper specimen material. Numbers correspond to the oscillation numbers.

Note that the numbers shown in the figures correspond to oscillation numbers in the calculation, not the actual ones.

Figure 11(c) shows the calculated largest dimensionless contact pressure for each position on the lower specimen in one oscillation of the upper specimen. The contact pressure was normalized by the specimen material hardness, which means the dimensionless contact pressure indicated 1 when the contact pressure reached the specimen material hardness. The contact pressure was "M"-shaped, and as a result, the wear depth was "W"-shaped as shown in **Figure 11(b)**. The peak contact pressure of "M"-shape increased with the number of oscillations. **Figure 11(d)** shows the time trend of the maximum and mean contact pressure. The maximum dimensionless contact pressure of 69-N load exceeded the value 1 as the oscillation number increased, while that of 39-N load never did. The mean contact pressure of both loads gradually decreased.

Since the excess of the contact pressure over the material hardness or a measure of material strength could cause the wear transition [19], the wear transition of 69-N load occurred when the maximum dimensionless contact pressure exceeded 1.

Figure 12 shows the calculated dimensionless equivalent contact radius, normalized by the upper specimen radius, at each position on the upper specimen in one stroke. The contact point moved from the right to the left in the figure as the upper specimen moved to the right. The contact radius of the rightmost and leftmost parts of the upper specimen decreased as the number of the strokes increased, indicating

Specimen radius	Upper specimen	3 mm
	Lower specimen	10 mm
Specific wear rate	10^{-1} mm^3/Nm	
Line load	34.5 N/mm	
Stroke	10 mm	
Δx	0.02 mm	
Number of points in moving average	17	

Table 3.
Calculation conditions [2].

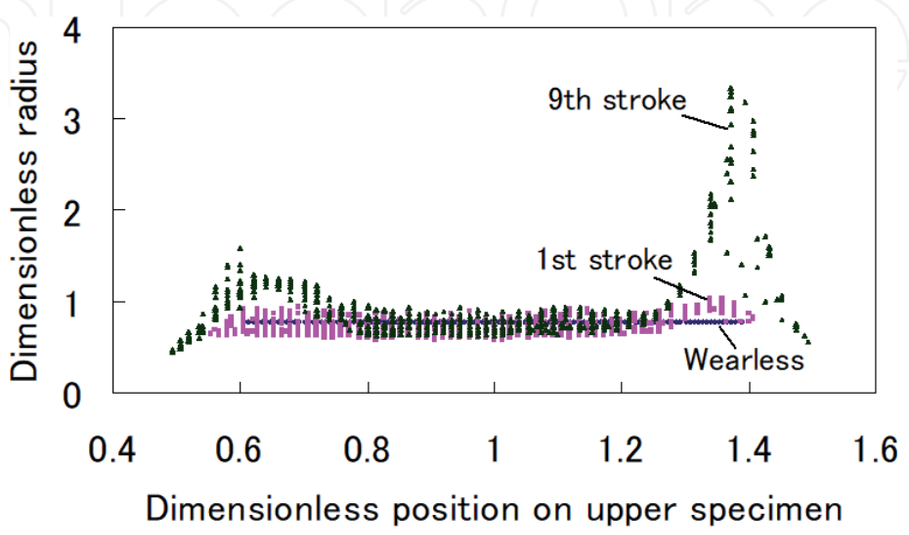

Figure 12.
Calculated dimensionless equivalent contact radius [1].

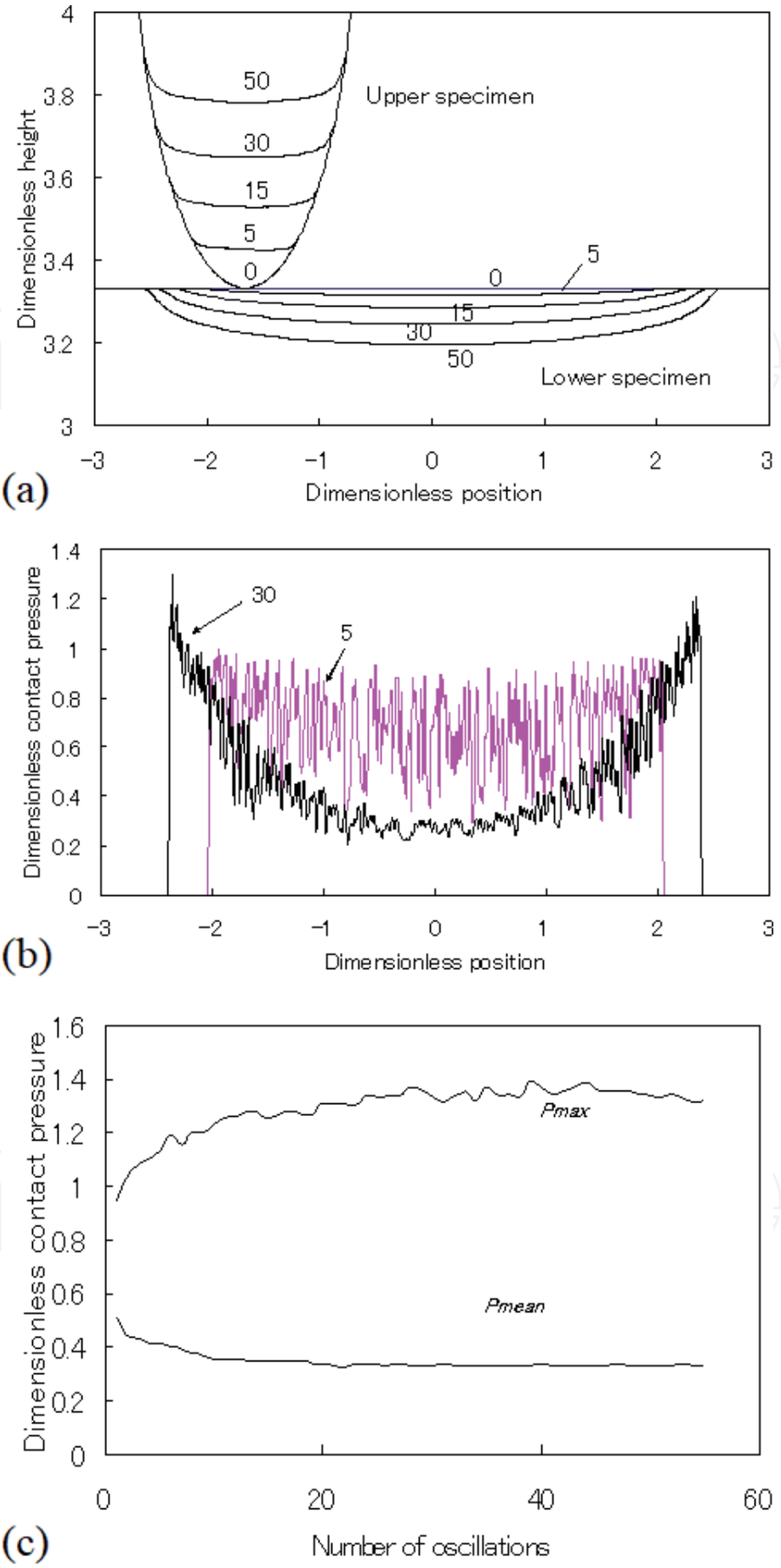

Figure 13.
Simulation results for a pure sliding pair of cylindrical upper specimen and flat plate lower specimen of 98-N load: (a) specimen's shape change, (b) contact pressure on the lower specimen, and (c) time trends of the contact pressure (symbols correspond to ***Figure 11****) [1].*

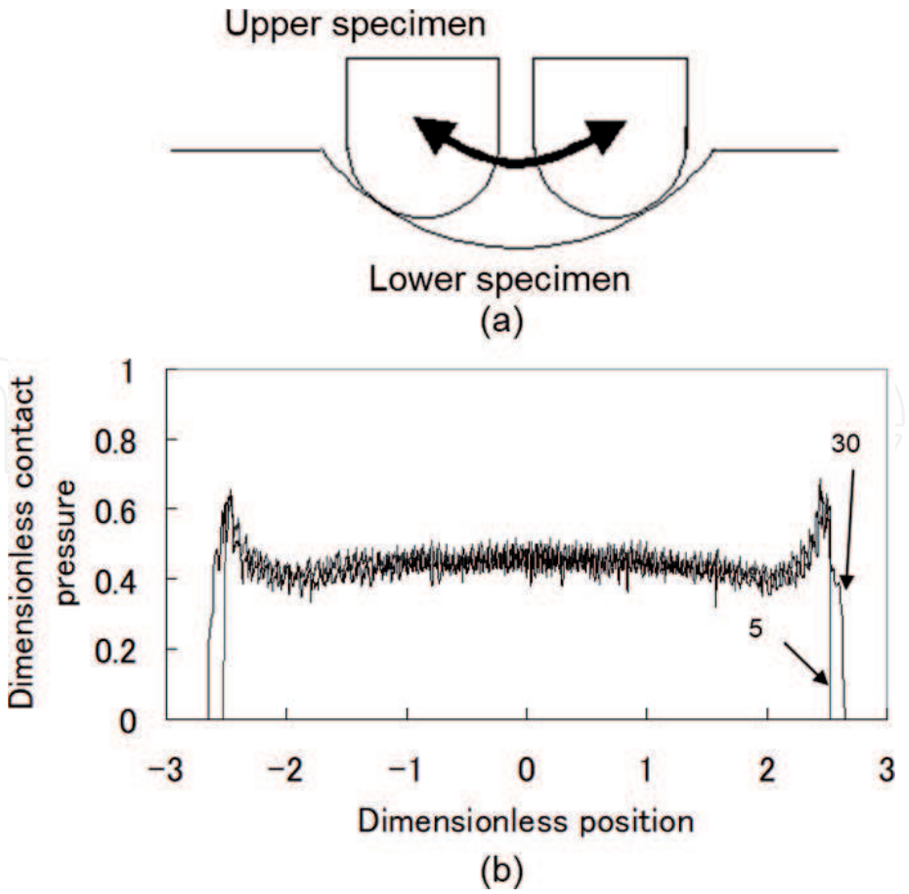

Figure 14.
*Motion and contact pressures for arc-concave lower specimen: (a) motion, (b) contact pressure (with symbols corresponding to **Figure 11**); concave radius: 10 mm (other conditions were the same as listed in **Table 1**.) [2].*

significantly smaller value than 1. This suggests that large contact pressure was generated by increasing inconformity of the contact surface shape.

As described in Section 2.1, the rolling-sliding motion of the sliding pairs in these experiments was the opposite of that often seen on machines, that is, the direction of the rolling and that of the sliding were opposite. In this rolling-sliding motion, a part that has once worn due to sliding may be returned to the contact portion again during one stroke due to the rolling motion. Perhaps this feature causes the inconformity of wear shapes leading to wear transition.

What about other shaped specimens? **Figure 13** shows the simulation results for a pure sliding pair of cylindrical upper specimen and flat plate lower specimen of 98-N load [1]. Dimensionless contact pressure exceeded 1, but its position was the end of the stroke. Therefore, the large contact pressure would have little effect for wear and caused no wear transition as shown in **Figure 2**.

Figure 14 indicates the simulation results for the cylindrical upper specimen and the arc-concave lower specimen of 34.5 N/mm line load (corresponding to 69-N load in **Figure 2**) [2]. As the direction of the rolling and that of the sliding was the same in the rolling-sliding motion for this sliding pair, the recontact of worn portion did not occur leading to lower contact pressure.

3. Characteristics of wear track profiles

3.1 Experimental

Pin-on-disk wear tests were carried out for some materials and under several conditions to obtain wear tracks to be compared and analyzed [11, 12]. The lower

part of the vertical set disk was immersed in mineral oil and the contact point with the pin was wetted along with the rotation of the disk. The pin had a flat surface of 8 mm diameter. The pin and the disk surface had a roughness of Ra ~0.3 micrometer. Test conditions and materials are shown in **Table 4**.

Figure 15 shows the wear track photos for the stainless and the brass disks tested in wet condition. Both indicated the streaked wear track and were difficult to discern visually, despite the different materials and test conditions. The wear tracks of the other specimens also showed the similar appearances. **Figure 16** indicates the examples of the wear track profiles. The valleys with 200–500 micrometer width and 20–70 micrometer depth were prominent and these similar dimensions of the valleys may bring the visual similarity of the wear tracks.

3.2 Characterization of wear track profiles

To evaluate the geometric similarity between the wear tracks quantitatively, frequency analysis was applied to the wear track profiles. Since the characteristics of the profile shape curve seems incidental rather than periodic, discrete wavelet transform (DWT) was applied. Details of the analysis were described in Ref. [11].

Figure 17 indicates the power spectral density (PSD) of DWT with regard to the wavelength of the roughness. Although there are some deviations, the PSD curves in the figure had almost the same shapes, that is, they had similar slopes and bended at about the same point, showing the geometrical similarity of the profiles. The profile shape curve of the wavelength at the bending point determines the rms

	Pin material	Disk material	Oil	Sliding velocity (m/s)	Load (N)	Sliding duration (h)
a	JIS S45C steel	JIS SUS304 stainless steel	Wet	0.02	118	1.68, 2, 8, 40, 80
b	JIS C3604 brass	JIS C3604 brass			54, 78, 118	20
c	JIS S45C steel	JIS SUS304 stainless steel	Dry		54, 78	2
	JIS S45C steel	JIS SUS304 stainless steel			118	1, 2, 4, 6

Table 4.
Test conditions and materials [11].

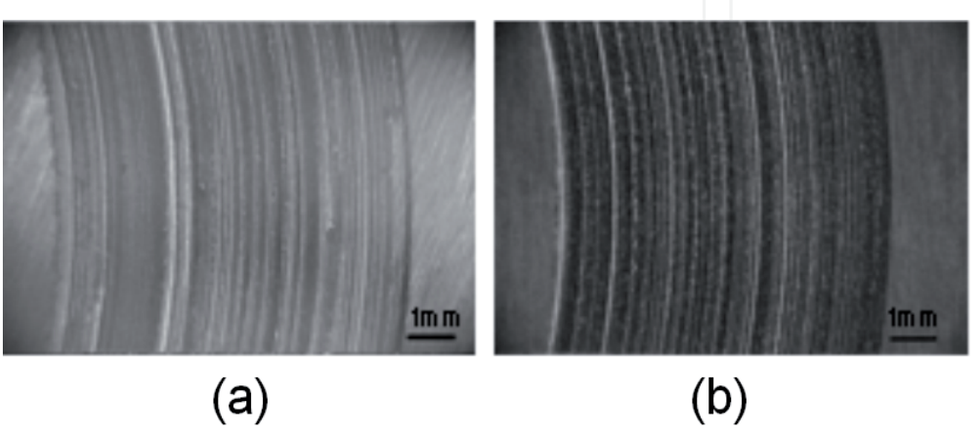

Figure 15.
Photos of typical wear tracks on disks: (a) SUS304 versus S45C, 118-N load, 8-h sliding and (b) C3604 versus C3604, 54 N, 20-h sliding [11].

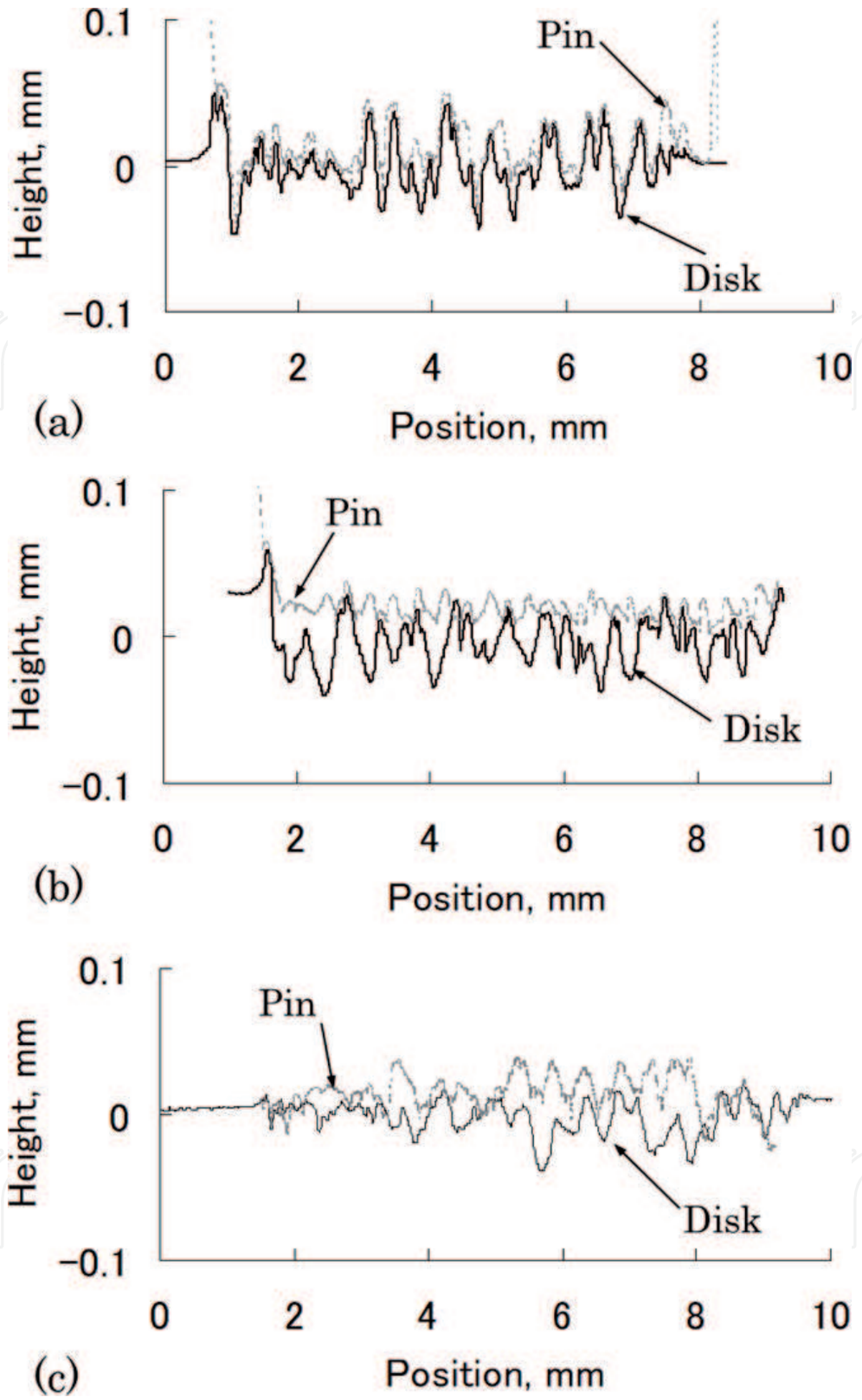

Figure 16.
Examples of combined wear track profiles for disks and pins: (a) S45C versus SUS304, 118-N load, 8 h, wet; (b) C3604 versus C3604, 54-N load, 20 h, wet; and (c) S45C versus SUS304, 118-N load, 4 h, dry [11].

roughness [20] and was visually conspicuous because valleys (or mountains) of the roughness larger than this wavelength had comparatively small depth to their width and were recognized as waviness.

In order to indicate the bending points explicitly, PSD ratios: $\ln\{P_W(\lambda_n)/P_W(\lambda_{n-1})\}$, where $P_W(\lambda_n)$ denotes the PSD at nth wavelength in **Figure 17**,

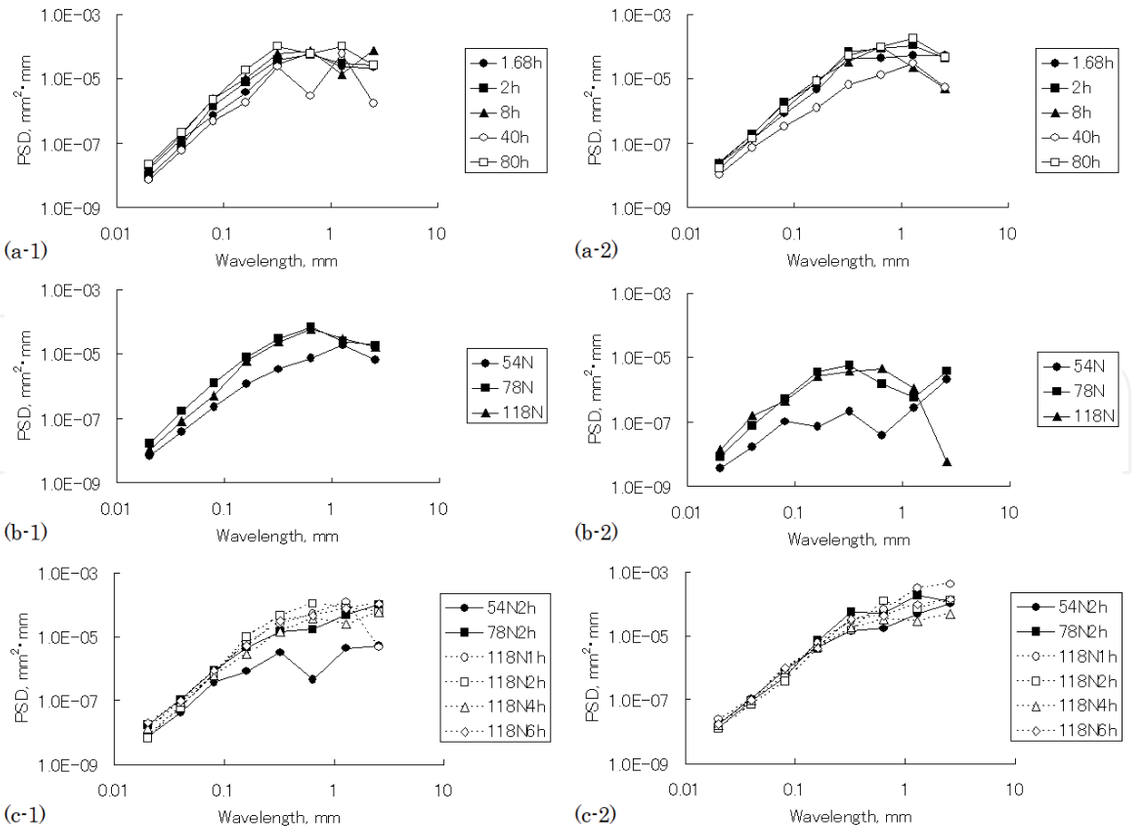

Figure 17.
Power spectral density (PSD) of DWT: (a) S45C versus SUS304, wet; (b) C3604 versus C3604, wet; and (c) S45C versus SUS304, dry, (−1) disks, (−2) pins [11]. Test conditions in (a) ~ (c) correspond to those of a ~ c in ***Table 4****.*

were calculated and shown in **Figure 18**. The PSD ratios showed sharp drops at the wavelength of 0.2–0.5 mm indicating the bending points. The PSD values at these wavelength were 10^{-5}–10^{-4} mm^2 •mm that were approximately equivalent to the valley depth of 30–80 micrometers. These results supported the above observations of valleys of the roughness that characterized the wear tracks.

3.3 Mechanism of generating wear track profiles

Pin-on-disk tests were used to capture the moment of the streak formation. The tester used was as the same as above. JIS S45C steel pins and JIS SUS304 stainless steel disks with surface roughness of Ra ~ 0.3 micrometer are used under 118-N load and wet conditions. The pin-disk assembly is shown in **Figure 19(a)**.

The disk rotation started slowly and then maintained a rotational speed of 12–13 rpm (sliding speed of ~0.03 m/s) to observe the wear track generation process. No signs of wear or damage were observed on the disk on the first few rotations, after which a groove appeared suddenly. As soon as the groove was found, the disk rotation was stopped. Other tests continued rotating after the first groove appeared. In each test, initially only one groove appeared, and after several rotations, the second groove appeared adjacent to the first groove, and so on, and the streak pattern was generated (sometimes, new groove generated at the other place to become another core of the streak).

Figure 19(b) and **(c)** shows the SEM images of the pin surfaces after testing. Transfer particles [21, 22] of about the same size were found on the pin surfaces that matched the number of grooves on the disks. Obviously, these transfer particles plowed the disk surface and generated the grooves of nearly the same size. The

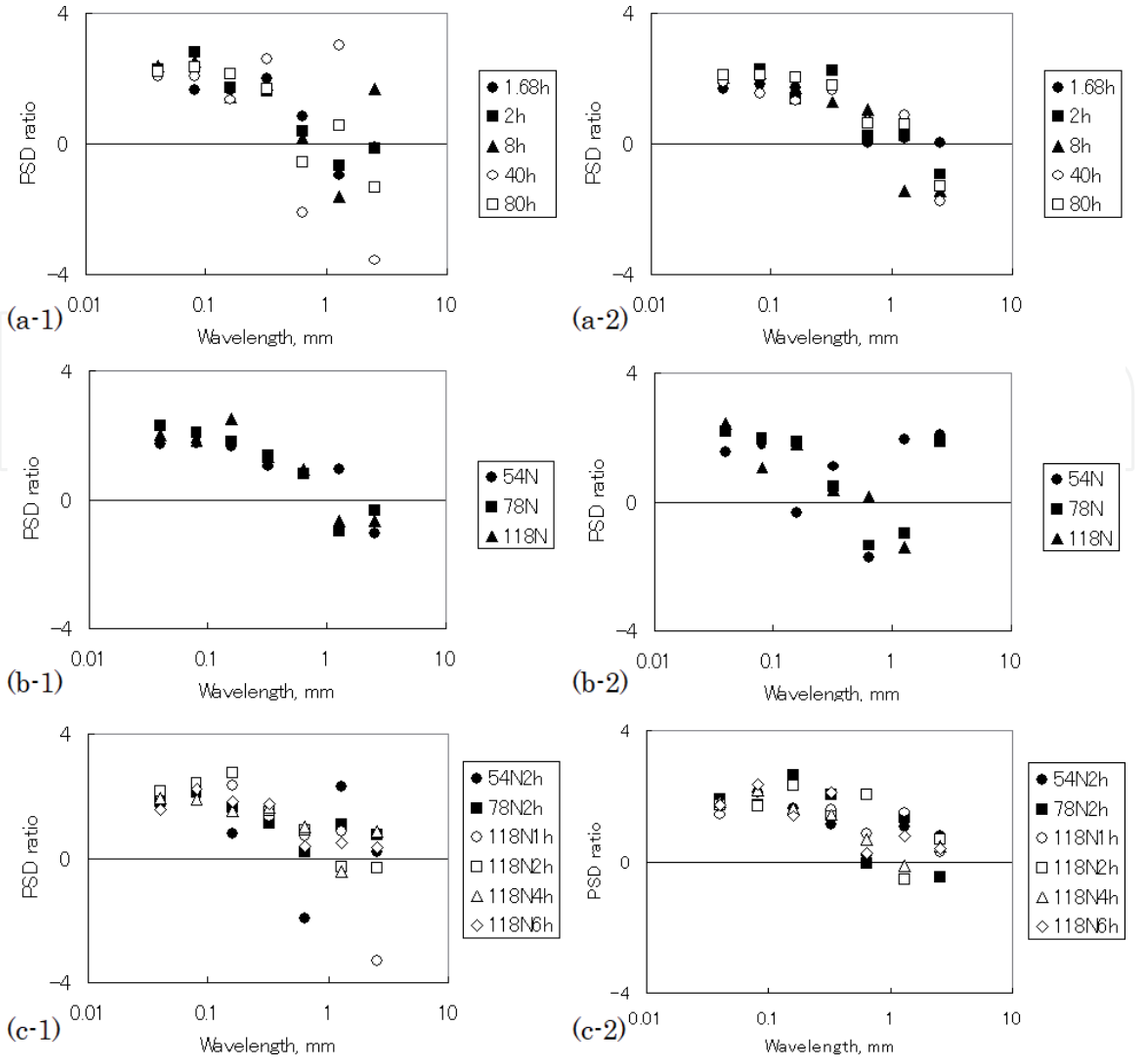

Figure 18.
PSD ratios [11]. Notations (a-1)–(c-2) correspond to those in ***Figure 17****.*

transfer particles included Cr, Ni and Fe according to the energy-dispersive X-ray spectroscopy analysis, suggesting that they originated in a mixture of both the pin and the disk materials and grew to and stopped growing at that size in that place.

Figure 20 shows the surface profiles of the tested pin and the disk. The measuring directions on the pin surfaces were shown in **Figure 19**. As seen in the SEM images, the sizes of transfer particles and naturally those of the grooves were similar and were in the range of the characteristic sizes above. This caused the similar appearances of the wear tracks.

Why were the transfer particles (and their resulting grooves) about the same size? From **Figure 20**, all grooves on the disks were found to have the ridges along their sides that dug into the pin surfaces. These ridges were also found for brass material [11]. These ridges digging into the mating surfaces enclosed the transfer particles and could be assumed to terminate their growth. Also, these ridges digging into the mating disk surface seems to generate the "counter" ridges on the disk and the counter ridges grew to dig into the pin surface generating a new seed of the transfer particle, as shown in **Figure 20(b)**.

3.4 Ridge formation conditions

We assumed that the ridges along the sides of the grooves have a key role to determine the characteristic scales of the wear track streaks and conducted the

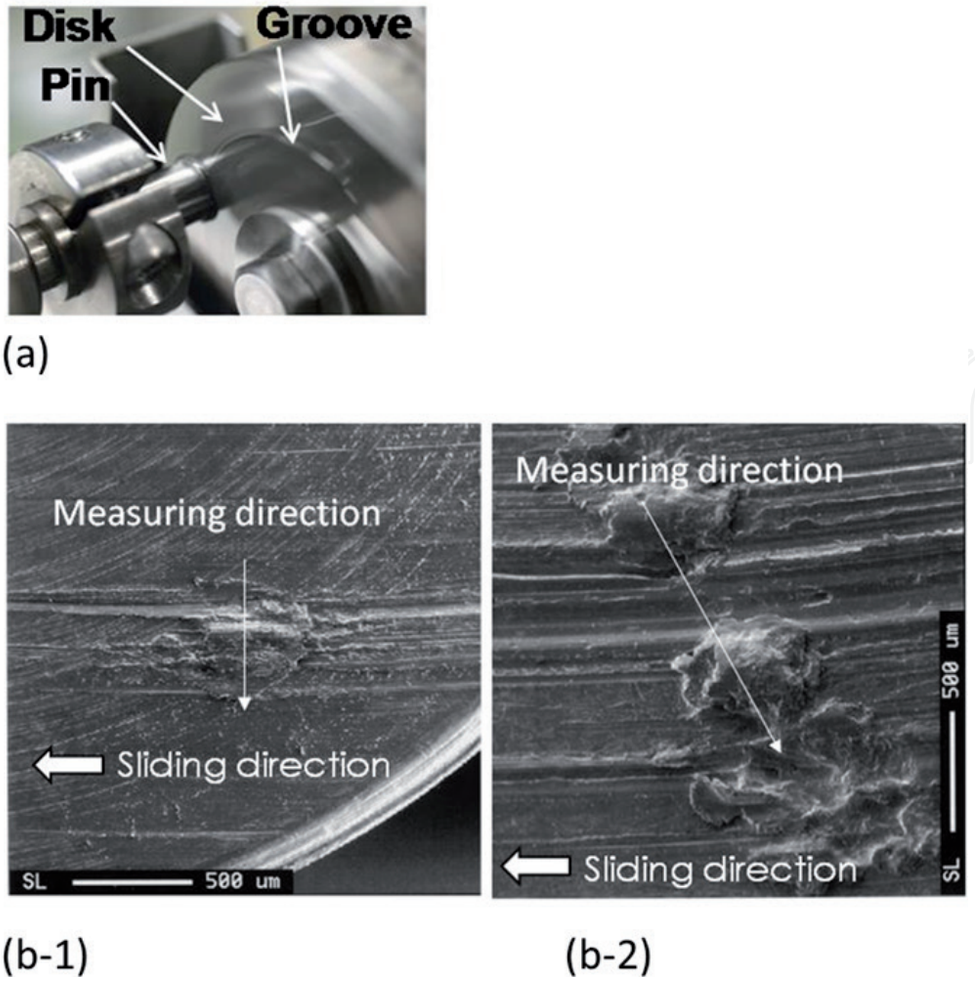

Figure 19.
Perspective of pin-disk assembly and SEM images of pin surfaces after the tests: (a) pin-disk assembly and (b-1) and (b-2) one and 2 transfer particles adhering to pin surfaces, respectively [12].

ridge formation tests. **Figure 21** shows the schematic of the test rig. Two metal plates sandwiched three hard balls and were pressed. Then one plate was rotated at an angle of 90°generating three grooves on the plate. The ball materials and the test conditions are listed in **Table 5**. Plate materials were JIS SUS304 stainless steel and JIS C3604 brass. Some tests were under oil-wetted conditions. The balls were fixed to one plate to prevent rolling in some cases.

Figure 22 shows the examples of groove profiles generated in the tests. You can see the groove with and without the ridge in the figure. **Figure 23** illustrates the groove profile. We designate $2d/\lambda_1$ in **Figure 23** as the "degree of penetration or D_p." The degree of penetration was originally defined as y/a in **Figure 24** for the wear map [23] and is approximately equivalent to $2d/\lambda_1$ in **Figure 23**. **Figure 25** shows the relations between D_p and h/d. In **Figure 25**, h/d is 0, that is, no ridge, for small D_p. h/d increased sharply when D_p exceeded about 0.05–0.1 regardless of the materials. This means that the valleys with higher aspect ratio (larger Dp) had higher ridges on their sides.

From the slopes of PSD curves in **Figure 17**, PSD values were proportional to about the third power of wavelength. This relation is replaced with the relation of $(\text{depth}) \propto (\text{width})^{1.5}$ in the valley profiles. Suppose the grooves grew during sliding maintaining this relation and "depth" and "width" were equivalent to d + h and λ_2, the relation of $d + h = 50 \times (\lambda_2/400)^{1.5}$ holds, when the typical value of d + h = 50 micrometer andλ_2 = 400 micrometer were used. The solid curve in **Figure 26** indicates this relation. The groove can be considered to grow along this curve.

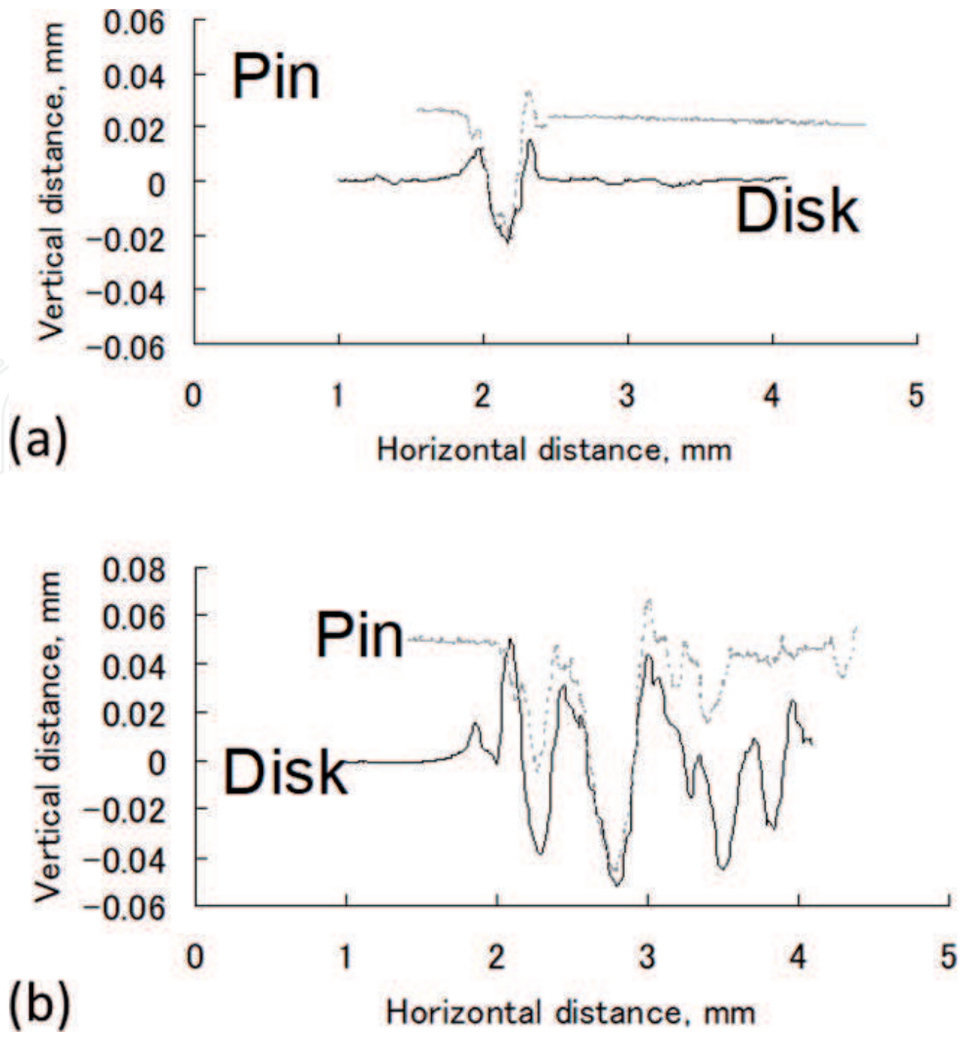

Figure 20.
Surface profiles of pins and disks [12]. Measuring directions of (a) and (b) correspond to those in ***Figure 1*** *(b-1) and (b-2), respectively.*

If the ridges began to form at $D_p = 0.1$, then $d = 0.05\lambda_1$. The dashed line in **Figure 26** indicates this relation. The intersecting point of the two lines indicates the time when the ridge began to form, the groove width at that time could be read as about 70 micrometers. The time when the ridge grew and dug into the mating surface was after this. Probably the groove width grew to a few 100 micrometers at that time, which was the characteristic scale of the grooves in the streaked wear track. We, therefore, consider this mechanism causes the wear track appearance similarity.

4. Conclusion

In this chapter, we have described two characteristic wear phenomena that are usually less noticeable, but we believe they characterize some aspects of wear and can serve as a background for examining various wear phenomena.

Mild-to-severe wear transition could occur for convex-shaped sliding pair due to their rolling-sliding motion which generates peculiar wear shapes leading to large contact pressure. Streaked wear track were shown to have a similar profile consisting of grooves with 200–500 micrometer width and 20–70 micrometer regardless of friction materials and conditions. This is because the transfer particles that plow the surface and produce grooves grow with sliding, but stop at about the same size, regardless of friction material and conditions.

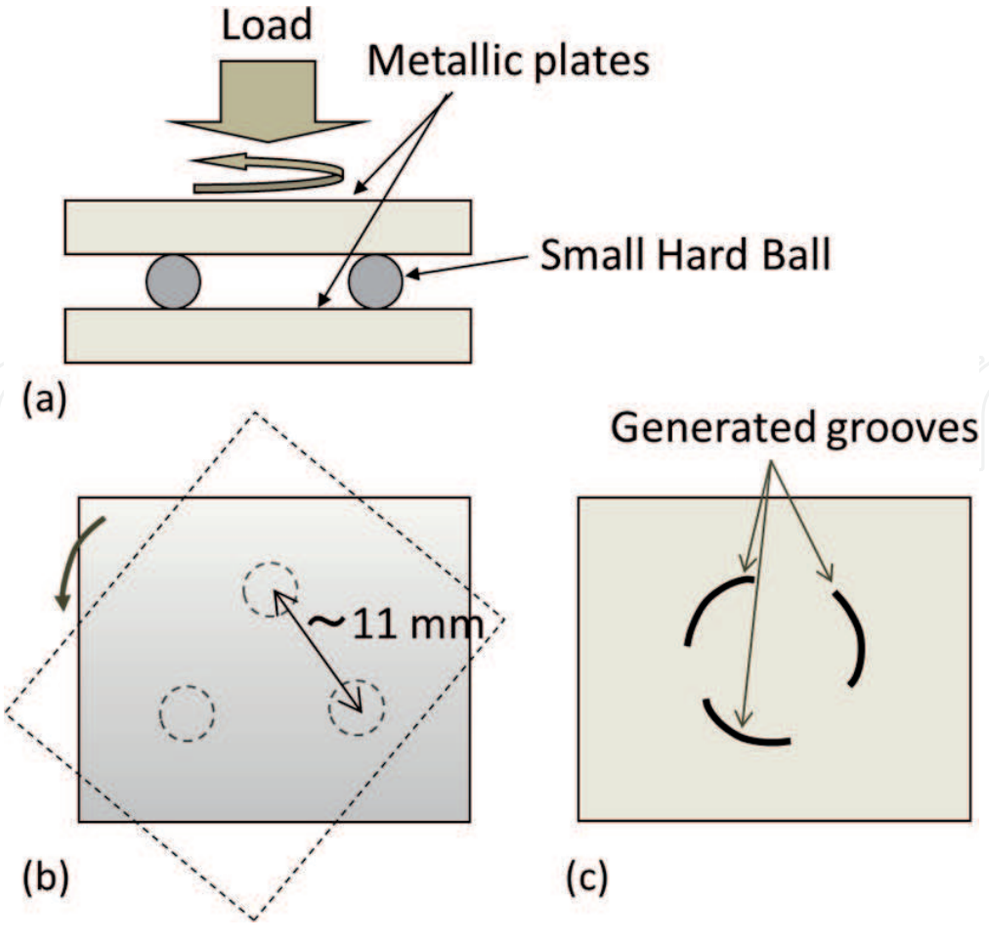

Figure 21.
Figure 3 *Schematic of ridge generating rig: (a) side view, (b) top view, and (c) generated groove trajectories [12].*

Ball material	Ball diameter (mm)	Load for 3 balls (N)
ZrO_2	0.1	15
	0.2	8, 30, 50
	0.5	100
	1	200
JIS SUS440C stainless steel	0.3	4, 15, 60, 100
JIS SUJ2 bearing steel	0.3	15, 60, 100
	0.5	60, 200, 300, 500
	1	20, 60, 200
	1.5	500
	2	500

Table 5.
Ball materials and test conditions [12].

Though we have not actually verified, we can consider the methods to prevent these wear damages. One of the methods to prevent the wear-induced mild-to-severe wear transition is, for example, to reduce the curvature of the surface to reduce the rolling-sliding motion and the contact pressure. One method to prevent the wear track generation is to prevent the transfer particle generation by effective lubrication

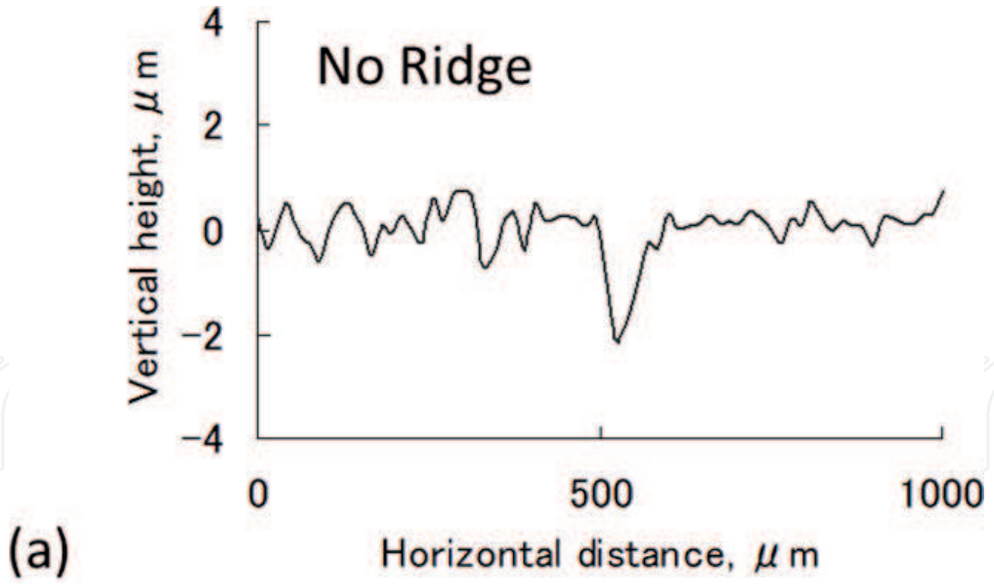

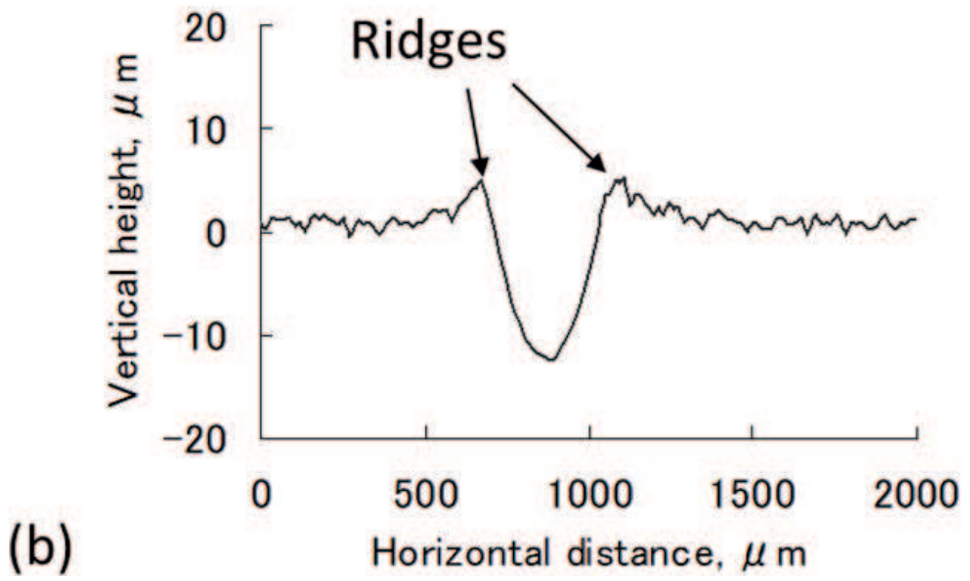

Figure 22.
Examples of measured groove profiles generated with ((a)) and without ((b)) ridges: (a) 0.3 mm in dia. SUJ-2 ball, 5 N/3 balls and (b) 2 mm in dia. SUJ-2 ball, 500 N/3 balls [12].

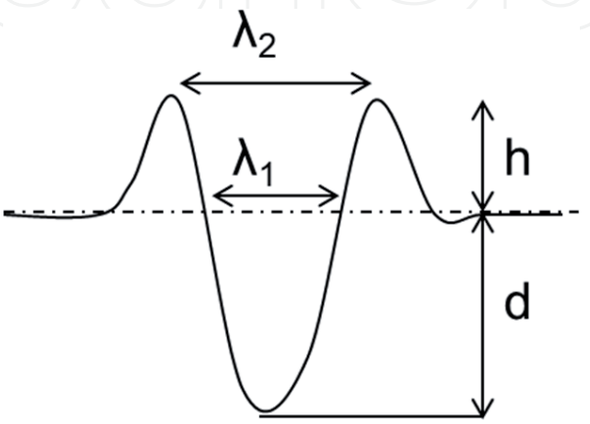

Figure 23.
Illustrated groove profile and notations of dimensions of groove and ridges [12].

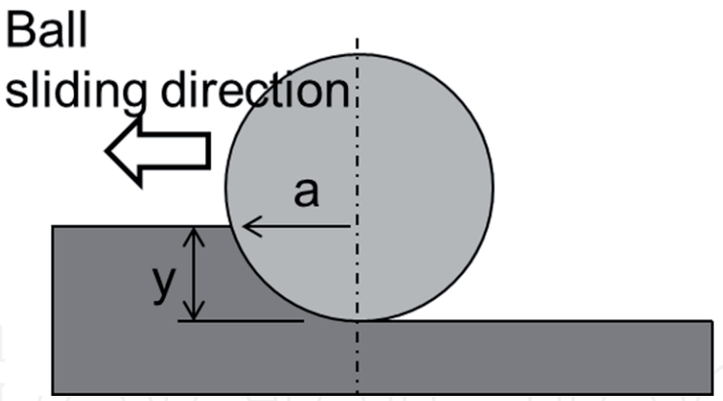

Figure 24.
Degree of penetration: y/a [12].

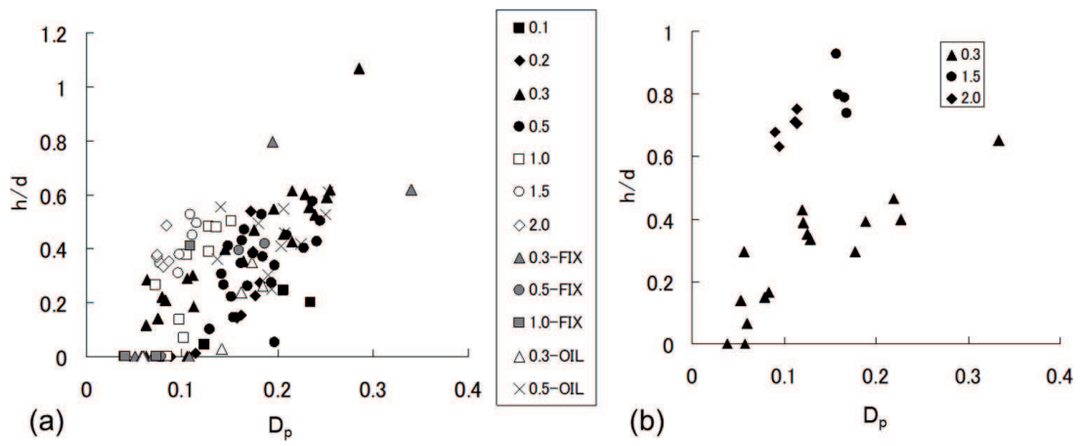

Figure 25.
Relations between Dp and ridge height rate h/d: (a) SUS304 plate and (b) C3604 plate [12]. Numbers, "FIX," "OIL" in boxes indicate ball diameter, using fixed ball, oil wetted conditions, respectively.

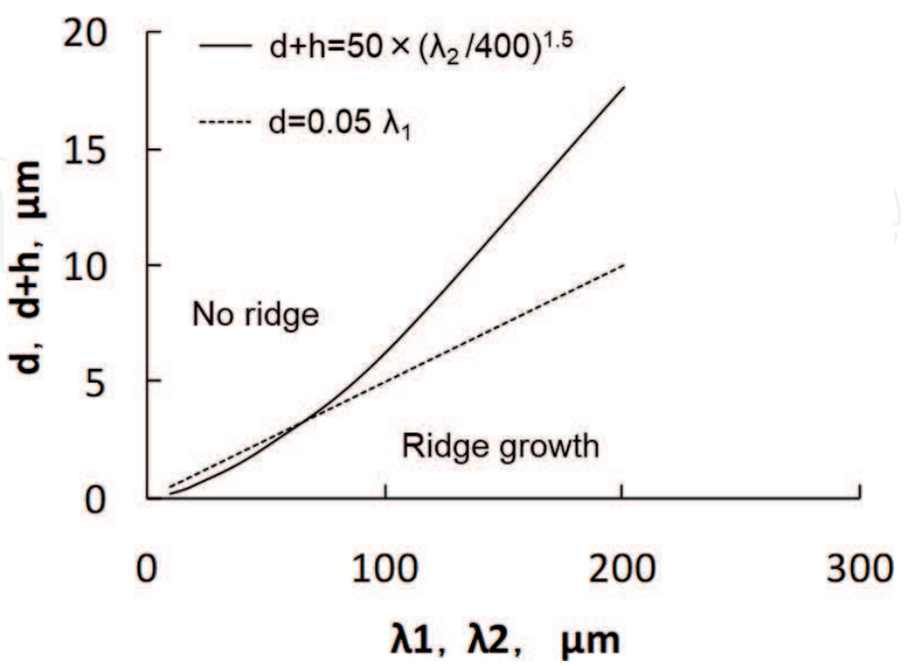

Figure 26.
Relations between calculated width and depth of groove [12].

(e.g., adding effective lubricant additives). These sounds obvious, but these may not have been understood well without understanding the phenomena above.

Considering these mechanisms above would offer some suggestions for reducing wear damages, however, the applicability of these mechanisms (such as for non-metallic materials) further need to be verified.

Notes

Most of the content of this chapter is based on Refs. [1, 2, 11, 12].

Author details

Naofumi Hiraoka
Institute of Technologists, Saitama, Japan

*Address all correspondence to: hiraoka@iot.ac.jp

References

[1] Hiraoka N. Time-dependent mild to severe wear transition in oscillation motion of cylindrical sliding pairs under boundary lubrication. Transactions of ASME, Journal of Tribology. 2002;**124**:822-828

[2] Hiraoka N. A study on mild-to-severe wear transition due to inconformity of wear-induced shape. Wear. 2005;**258**:1531-1535

[3] Hanief M. Effect of surface roughness on wear rate during running-in of En31-steel: Model and experimental validation. Materials Letters. 2016;**176**:91-93

[4] Hu Y, Meng X, Xie Y. A computationally efficient mass-conservation-based, two-scale approach to modeling cylinder liner topography changes during running-in. Wear. 2017;**386-387**:139-156

[5] SMITH AF. The influence of surface oxidation and sliding speed on the unlubricated wear of 316 stainless steel at low load. Wear. 1985;**105**(2):91-107

[6] Garbar II. Gradation of oxidational wear of metals. Tribology International. 2002;**35**(11):749-755

[7] Korkut MH. Microstructure and wear behavior of Al2024\SiFe and Al2024\SiFe\Al2O3 composites. Tribology International. 2003;**36**(3):169-180

[8] Feser T, Stoyanov P, Mohr F, Dienwiebel M. The running-in mechanisms of binary brass studied by in-situ topography measurements. Wear. 2013;**303**(1-2):465-472

[9] Perez E, Tanaka M, Jibiki T. Wear of stainless steels—Cause and transition of wear of martensitic stainless steel. Marine Engineering. 2013;**48**(5):662-669

[10] Hayashi K, Hirasata K, Kamenaka Y, Augita K. Friction and wear of cast iron under high sliding speed and high contact pressure. 2nd report. The condition of the transition from mild wear to severe wear. Transactions of JSME C. 1997;**63**(616):4322-4327

[11] Hiraoka N, Matsumoto H. Characteristic scales of wear track profiles generated by pin-on-disk wear tests. Tribology Online. 2008;**3**(3):205-210

[12] Hiraoka N, Yamane E. A study on the mechanism of generating wear track grooves. Tribology Letters. 2011;**41**:479-484

[13] Nakano T, Hiratsuka K, Sasada T. Fractal analysis of worn surface and wear particles. Journal of Analytical Science and Technology. 1990;**35**:151-154

[14] Iliuc I. Plate-like wear particle formation in a lubricated ball-on-plate friction pair. Tribology International. 1985;**18**:215-221

[15] Flodin A, Andersson S. Simulation of mild wear in helical gears. Wear. 2000;**241**:123-128

[16] Olofsson U, Andersson S. Simulation of mild wear in boundary lubricated spherical roller thrust bearings. Wear. 2000;**241**:180-185

[17] Ovist M. Numerical simulations of mild wear using updated geometry with different step size approaches. Wear. 2001;**249**:6-11

[18] Flodin A, Andersson S. A simplified model for wear prediction in helical gears. Wear. 2001;**249**:282-285

[19] Samuels B, Richards MN. The transition between mild to severe wear for boundary-lubricated steels.

Transactions of the ASME, Journal of Tribology. 1991;**113**:65-72

[20] Persson BN, Tartaglino U, Volokitin AI, Albohr O, Tosatt E. On the nature of surface roughness with application to contact mechanics, sealing, rubber friction and adhesion. Journal of Physics. Condensed Matter. 2005;**17**:R1-R62

[21] Sasada T, Norose S, Tomaru M, Mishina H. The intermittent transversal movement of the rubbing surfaces by interposed wear particles. Junkatsu. 1978;**23**:519-526

[22] Norose S, Sasada T. The mutual transfer of rubbing materials and the mixing structure of wear particles formed in lubricating oil. Junkatsu. 1979;**24**:226-230

[23] Hokkirigawa K, Kato K. An experimental and theoretical investigation of ploughing, cutting and wedge formation during abrasive wear. Tribology International. 1988;**21**:51-57